Journal of Materials Chemistry A

Thick and Freestanding MXene/PANI Pseudocapacitive Electrodes with Ultrahigh Specific Capacitance

Journal:	*Journal of Materials Chemistry A*
Manuscript ID	TA-ART-06-2018-005807.R1
Article Type:	Paper
Date Submitted by the Author:	17-Jul-2018

Complete List of Authors:	VahidMohammadi, Armin; Auburn University, Materials Engineering Moncada, Jorge; Auburn University, Chemical Engineering Chen, Hengze; Auburn University, Materials Engineering Kayali, Emre; Auburn University, Materials Engineering Orangi, Jafar; Auburn University, Materials Engineering Carrero, Carlos A.; Auburn University, Chemical Engineering Beidaghi, Majid; Auburn University, Materials Engineering

Thick and Freestanding MXene/PANI Pseudocapacitive Electrodes with Ultrahigh Specific Capacitance

Armin VahidMohammadi [1], Jorge Moncada [2], Hengze Chen [1], Emre Kayali [1], Jafar Orangi [1], Carlos A. Carrero [2], Majid Beidaghi [1,*]

[1] Department of Mechanical and Materials Engineering, Auburn University, Auburn, AL 36849, USA

[2] Department of Chemical Engineering, Auburn University, Auburn, AL 36849, USA

* Corresponding author: mbeidaghi@auburn.edu

Abstract

Two-dimensional (2D) titanium carbide MXene ($Ti_3C_2T_x$) has shown great promise as a high-performance electrode material for electrochemical capacitors (ECs). However, similar to other 2D materials, processing MXenes into freestanding films results in their restacking, decreasing ion transport inside the electrodes. This problem significantly hinders the specific capacity and rate capability of freestanding electrodes, particularly for those with thicknesses higher than a few microns. Here, we demonstrate a strategy based on surface modification of MXene sheets to fabricate electrodes with highly accessible structure and improved electrochemical performance even at very high electrode thicknesses. 2D $Ti_3C_2T_x$ and polyaniline (PANI) hybrid materials were synthesized through oxidant-free *in situ* polymerization of PANI on surface of MXene sheets and were assembled into freestanding films with various thicknesses. Thin MXene/PANI hybrid electrodes delivered outstanding gravimetric and volumetric capacitances as high as 503 F g^{-1} and 1682 F cm^{-3}. As the electrode thicknesses and mass loadings were increased, the hybrid electrodes still showed high electrochemical performance. For example, an electrode with a thickness of 90 µm and mass loading of 23.82 mg cm^{-2} could deliver a specific capacitance of about 336 F g^{-1} (~888 Fcm^{-3} volumetric capacitance). The hybrid electrodes also showed a high cycle lifetime with a capacitance retention of 98.3% after 10,000 cycles. This paper explains a simple and fast approach for fabrication of MXenes/conducting polymer hybrid electrodes with superior electrochemical performance.

Keywords: MXene, $Ti_3C_2T_x$, 2D materials, polyaniline, pseudocapacitance, supercapacitors.

1. Introduction

Development of energy storage devices with high power and energy densities, such as advanced batteries and electrochemical capacitors (ECs, also called supercapacitors), is crucial for the future advancement of portable electronics, electric vehicles, and grid-scale energy storage.[1–3] ECs are electrochemical energy storage devices with long lifetime and fast charge and discharge capabilities and therefore, can complement or replace batteries in applications with high power requirement.[4–6] Two-dimensional (2D) materials are among the most promising electrode materials for advanced ECs. Due to their high surface-area-to-volume ratios, 2D materials offer an abundance of active surface area for charge storage through electric double layer capacitance (EDLCs) or fast surface redox reactions (pseudocapacitance).[7] 2D transition metal carbide and nitrides, collectively referred to as MXenes, are an emerging family of 2D materials with unique physical and chemical properties. MXenes have received considerable attention for applications such energy storage,[4,8–11] gas-sensing,[12,13] electromagnetic interference shielding,[14] and capacitive deionization,[15] to name a few. With a general formula of $M_{n+1}X_nT_x$ (n=1, 2, and 3), where M stands for a transition metal, X is carbon and/or nitrogen, and T_x represents different surface functional groups,[16–19] about 20 different MXene compositions and structures are synthesized so far and many more are theoretically predicted.[7] $Ti_3C_2T_x$ is the first discovered and the most studied MXene which is synthesized by selective removal of Al atoms from structure of Ti_3AlC_2, a member of a family of layered ternary carbides and nitrides called MAX phases.[16] $Ti_3C_2T_x$ is a highly conductive 2D material with a functionalized surface that enhances participation of Ti atoms in the fast redox reactions.[8] As a result, $Ti_3C_2T_x$ shows an exceptional performance as an electrode material for ECs.[4,7,8,20]

An advantage of 2D materials, such as MXenes, over the conventional EC electrode materials is that they can be assembled into freestanding and flexible electrodes and devices using simple and binder-free fabrication methods (e. g. vacuum filtration and layer-by-layer depositions). Previous studies on the fabrication and evaluation of freestanding MXene electrodes have shown that thin $Ti_3C_2T_x$ electrodes can deliver specific capacitances as high as 450 F g^{-1}.[8,20,21] However, similar to the other 2D materials, MXene sheets tend to restack during electrode fabrication, which severely reduces the ion transport in the structure of the electrode. This problem is more pronounced in the case of thicker electrodes and, as a result, freestanding electrodes

fabricated by direct assembly of the 2D sheets usually show highly thickness-dependent performances.[20] Restacking significantly affects the rate capability of $Ti_3C_2T_x$ electrodes and limits their charge storage capacity to far below the theoretical value of ~ 615 C g^{-1}.[8,22–25] To overcome this problem, various approaches have been applied to engineer the structure of the MXene electrodes and improve their ion transport properties. These include fabrication of microporous and hydrogel $Ti_3C_2T_x$ films[8] and designing hybrid electrodes of $Ti_3C_2T_x$ and carbon nanomaterials such as carbon nanotubes (CNTs)[21] and graphene.[25,26] While some of these strategies are effective in improving ion transport and high-rate electrochemical performance of the electrodes, they often reduce the electrode density resulting in decreased volumetric capacitance, rate capability, and energy density of the electrodes, particularly at higher electrode thicknesses.[8,25]

Recently, it has been demonstrated that the electrochemical properties of freestanding MXene electrodes can be improved by deposition of conductive polymers such as polypyrrole (PPy) and Poly(3,4-ethylenedioxythiophene) (PEDOT) on the surface of MXene sheets. Hybrid electrodes of $Ti_3C_2T_x$ and PPy have shown to deliver specific capacitances as high as 416 F g^{-1} in 1M H_2SO_4.[27] The performance of the electrodes fabricated using PEDOT deposited $Ti_3C_2T_x$ sheets were also improved compared to the electrodes fabricated using pristine $Ti_3C_2T_x$.[28] The improved performance of these hybrid electrodes does not stem from the contribution of the polymers to charge storage. PPy and PEDOT are both electrochemically inactive in the potential range that $Ti_3C_2T_x$ shows its highest electrochemical activity in acidic aqueous electrolytes (-0.7 V to +0.2 V vs. Ag/AgCl). In other words, in these cases, the deposited polymers only act as conductive spacers that prevent restacking of $Ti_3C_2T_x$ sheets in the electrode structure. This is a unique application of conductive polymers in designing high performance electrodes as these materials are more often considered as the active materials in various electrochemical energy storage systems.[29–31] However, previous studies have not fully explored this interesting electrode design strategy. For example, the effects of polymer loading in the hybrid electrodes and the thickness of the deposited polymer on electrochemical performance have not been investigated. In addition, the application of hybrid $Ti_3C_2T_x$/polymer sheets in designing high performance freestanding electrode with very high thicknesses has not been reported either.

Here, we report a design strategy for fabrication of hybrid electrodes of delaminated $Ti_3C_2T_x$ MXene and polyaniline (PANI) with outstanding electrochemical performances. Hybrid $Ti_3C_2T_x$/PANI sheets were synthesized by *in situ* and oxidant-free polymerization (i. e., without use of additional oxidizing chemicals) of aniline monomers on the surface of single-layer $Ti_3C_2T_x$ sheets. We show that controlling the amount of deposited polymer is a critical parameter affecting the electrochemical performance of the electrodes. By minimizing the amount of polymer deposited on the surface of $Ti_3C_2T_x$ flakes, we were able to design and fabricate electrodes with high ion transport properties and improved high-rate electrochemical performance compared to previously reported electrodes based on MXenes. An important advantage of the produced hybrid electrodes compared to pristine $Ti_3C_2T_x$ electrodes is that they can be fabricated in very high thicknesses without significant adverse effects on their electrochemical performance. For example, a 13 µm thick $Ti_3C_2T_x$/PANI hybrid film with a mass loading of 3.3 mg cm^{-2} delivered specific capacitances as high 458 F g^{-1} and 1163 F cm^{-3}, a performance similar to thin $Ti_3C_2T_x$ electrodes while maintaining a better rate-capability at higher scan rates compared to them. When the thickness of the hybrid electrodes was increased to 90 µm, they still showed acceptable specific capacitances and rate capabilities.

2. Experimental Section

MAX Phase and MXene Synthesis. Ti_3AlC_2 MAX phase was synthesized according to previous reports in the literature.[4] In summary, Ti_2AlC (Mesh ~400) and TiC (99.5%, ~ 2 microns, Alfa Aesar) powders were mixed in a 1:1 molar ratio and ball milled for 24h using zirconia grinding balls. The ball milled powders were then heated to 1400 ºC in a tube furnace under a flowing argon atmosphere at a heating rate of 5 ºC/min and were kept there for 2 hrs. Synthesized bulk Ti_3AlC_2 was milled using titanium carbide tips and sieved through a 400 mesh to obtain powders with an average particle size of ~32 microns. Ti_2AlC powder was prepared using a similar process with mixing TiC, Ti, and Al powders in 0.85:1.15:1.05 molar ratio, followed by 24h of ball milling, and heating at 1400 ºC for 4h.

$Ti_3C_2T_x$ MXene was prepared according to the minimally intensive layer delamination (MILD) method.[32,33] Typically, 1g LiF (98.5%, Alfa Aesar) was added to 20 mL solution of 6 M HCl (ACS grade, BDH). The solution was stirred until the LiF powder was completely dissolved. Then 1g of Ti_3AlC_2 MAX phase powder was slowly added to the LiF-HCl etching solution (in

over ~10 minutes). An ice bath was used to dissipate the excess heat from the etching solution while adding the MAX phase powder. The solution was continuously stirred at 550 rpm using a Teflon coated magnetic bar for 24h at 35 ºC. The etched powder was then washed several times by DI water, hand-shaken for at least 1 minute, and centrifuged at 3500 rpm for 5 minutes until obtaining a dark green supernatant or when the pH of the supernatant became higher than 5. At this point, etched particles were probe sonicated (with 35% amplitude/~250 W power) in deaerated DI water (~1g powder in 200 mL water) for 1h. Again, an ice bath was used to avoid excessive heat generation and oxidation of MXene during probe sonication. The final solution (referred to as $Ti_3C_2T_x$ MXene solution in the text) was obtained by centrifugation of the sonicated powders at 3500 rpm for 1h. The concentration of resulting MXene solutions was calculated by filtering a known volume of solution and measuring the weight of the resulting freestanding $Ti_3C_2T_x$ film after it was completely dried.

$Ti_3C_2T_x$*/PANI Hybrid Electrodes Preparation*. To prepare the MXene/PANI hybrids, first 300 µL of aniline monomer (99+%, Alfa Aesar) was dissolved in 20 mL solution of 1M HCl. Then, the aniline/HCl solution was slowly added to a dispersion $Ti_3C_2T_x$ in water (with the desired aniline to MXene weight ratio), and the mixture was stirred for 10 minutes. The addition of aniline/HCl solution to the MXene dispersion resulted in the precipitation and crumpling of $Ti_3C_2T_x$ sheets after absorption of aniline. The prepared solutions with different MXene to aniline ratios were sealed and kept at ~ 4 ºC for 5h. The final solutions were centrifuged at 3500 rpm for 1 minute and washed with DI water two times to remove any residual and unreacted aniline monomer. Each time 45 mL of water was added to the centrifuge tube and after the centrifugation the obtained clear supernatant was decanted. After the final wash, $Ti_3C_2T_x$/PANI hybrid sheets were dispersed in ~30 mL DI water by handshaking and the dispersion was filtered on a Celgard® membrane filter to fabricate freestanding MXene/PANI hybrid films. The hybrid films were punched into desired sizes and were directly used as electrodes for electrochemical measurements.

Electrochemical Measurements. All electrochemical experiments were carried out by a BioLogic VMP3 potentiostat in a three-electrode setup using Swagelok cells (Fig. S3). In stainless steel (SS) Swagelok cells (used for early experiments done in narrow voltage window, please see electronic supplementary information-ESI), SS rods were used as current collectors, and in plastic Swagelok cells, glassy carbon rods were used as current collectors for both working and counter electrodes. In all experiments, Ag/AgCl immersed in 1M KCl and an overcapacitive activated

carbon (YP-50) were used as the reference and counter electrodes, respectively. To prepare the counter electrode, a mixture of 95 wt.% activated carbon 5 wt.% PTFE was dispersed in ethanol and stirred at 45 ºC until most of the ethanol was evaporated. The resulting thick slurry was then rolled into freestanding films and punched to be used in the electrochemical cells. The working electrode was prepared by punching the filtered MXene and MXene/PANI films. In all experiments, the electrolyte was 3M H_2SO_4 solution and two layers of Celgard® membranes were used as separators. Cyclic voltammetry (CV) experiments were performed at scan rates ranging from 2 mV s^{-1} to 10 V s^{-1} in a -0.7 V to +0.2 V potential window (vs. Ag/AgCl). All cells were first pre-cycled for 50 times at scan rate of 20 mV s^{-1} before any further measurements. To evaluate the cyclic performance of the electrodes, CV experiments were carried out at a scan rate of 20 mV s^{-1} over 10,000 cycles. Galvanostatic charge/discharge experiments were performed between -0.7 V to +0.2 V (V vs. Ag/AgCl) at current densities of 5, 10, 20, 30, and 50 A g^{-1}. The capacitance of the electrodes was calculated from the CV graphs by using the following equation:[20]

$$C = \frac{1}{\Delta V}\int \frac{j\,dV}{s} \qquad (1)$$

where C is the normalized capacitance (F cm^{-3} or F g^{-1}), j is the current density (mA cm^{-3} or mA g^{-1}), V is the voltage (V), ΔV is the voltage window (V), and s is the scan rate (mV s^{-1}).

Symmetric cells were assembled by using $Ti_3C_2T_x$/PANI electrodes as the both working and counter electrodes. The specific power (P) and energy (E) densities were calculated as follow:[4]

$$E = (\frac{1}{2} \times C \times V^2) / 3600 \quad [\text{Wh L}^{-1}] \text{ or } [\text{Wh kg}^{-1}] \qquad (2)$$

$$P = E \times \frac{s}{V} \times 3600 \quad [\text{W L}^{-1}] \text{ or } [\text{W kg}^{-1}] \qquad (3)$$

Where C is the normalized capacitance of the cell (F cm^{-3} or F g^{-1}), V is the operating potential window (V), and s is the scan rate (V/s).

The contribution of diffusion-controlled and surface-controlled mechanisms in charge storage of the electrodes was calculated considering the power-law relationship between current, i, and scan rate, v ($i=av^b$). In short, the CV current value at each potential was divided to two different portions of capacitive controlled and diffusion controlled according to the following equation:

$$i(V) = k_1 v + k_2 v^{0.5}$$

where V is the potential and k_1 and k_2 are variables. $k_1\nu$ indicates the capacitive contribution (b=1 in the power-law relationship) and $k_2\nu^{0.5}$ is related to the contribution of diffusion-limited processes.

Materials Characterization Techniques. Structure and morphology of the synthesized MXene and MXene/Polymer hybrid films were characterized using a Bruker X-ray diffractometer (40 kV and 40 mA Cu-kα radiation) and JEOL JSM-7000F scanning electron microscope (SEM) equipped with an energy dispersive spectrometer (EDS). XRD analysis was done directly on the freestanding MXene films with a scan speed of 2 degrees/min. To investigate the polymerization of aniline monomer on $Ti_3C_2T_x$ nanosheets, Fourier transform infrared spectroscopy (FTIR) measurements were carried out using Perkin Elmer spectrum 100 ATR-FTIR spectrometer with a resolution of 4 cm^{-1}. Raman measurements were performed using a Renishaw InVia Qontor Raman Spectrometer with a 532-nm laser as the excitation source. For all measurements a 2400 L mm^{-1} grating was used in a range of 100–3200 cm^{-1} using a 100x long-distance objective lens. The spectra were recorded using 10% of the laser power, an exposure time of 10 seconds, and 10 accumulations for each spectrum. Thermogravimetric analysis (TGA) was performed using a TA instruments Q50 under O_2 atmosphere. First the temperature was ramped up to 120 ºC with a heating rate of 10 ºC/min and the sample was kept at this temperature for 30 min to evaporate all the moisture. Then, the sample was heated up to 800 ºC with the same rate and was hold at that temperature for 45 min. Atomic force microscope (AFM) measurements were carried out by Park Instruments NX10 AFM using a non-contact mode cantilever. AFM samples were prepared by drop casting diluted MXene solutions on silicon wafers or immersing silane-coated silicon wafers in well-dispersed and diluted solutions of $Ti_3C_2T_x$ or $Ti_3C_2T_x$/PANI.

3. Results and Discussions

The chemical deposition of PANI on a substrate or on the surface of different materials usually follows an oxidative polymerization process, where an oxidizing agent, such as ammonium persulfate (APS), is used to initiate the polymerization process.[2,34–36] The protonation of nitrogen atoms in the deposited polymer and its doping with anions (such as Cl^-) are important for achieving high quality conductive PANI through chemical deposition methods.[34] However, as explained further below, during our initial studies in this work, we found that aniline can spontaneously polymerize on surface of $Ti_3C_2T_x$ sheets even in the absence of an oxidant. This is in agreement

with previous reports that have shown oxidant-free deposition of PPy and PEDOT on $Ti_3C_2T_x$ nanosheets.[27,28] Chen et al. used a combination of experimental and theoretical studies to show that 3,4-ethylene dioxythiophene (EDOT) monomer can polymerize on surface of MXene as long as a charge transfer occurs between the monomer and MXene and the energy cost for polymerization decreases as the charge loss from monomer increases.[27,28] Fig. 1a schematically shows the process used for synthesis of $Ti_3C_2T_x$ and $Ti_3C_2T_x$/PANI hybrids. First, a dispersion of delaminated $Ti_3C_2T_x$ (d-$Ti_3C_2T_x$) flakes in water was prepared by selective removal of Al from the structure of Ti_3AlC_2 MAX phase in an etching solution composed of LiF and HCl. PANI was deposited on the synthesized MXene sheets by adding a solution of aniline dissolved in 1M hydrochloric acid (HCl).

As shown in Fig. 1b, after the gradual addition of the prepared solution to $Ti_3C_2T_x$ dispersion, the absorption of aniline by MXene flakes and their crumpling due to low pH of the

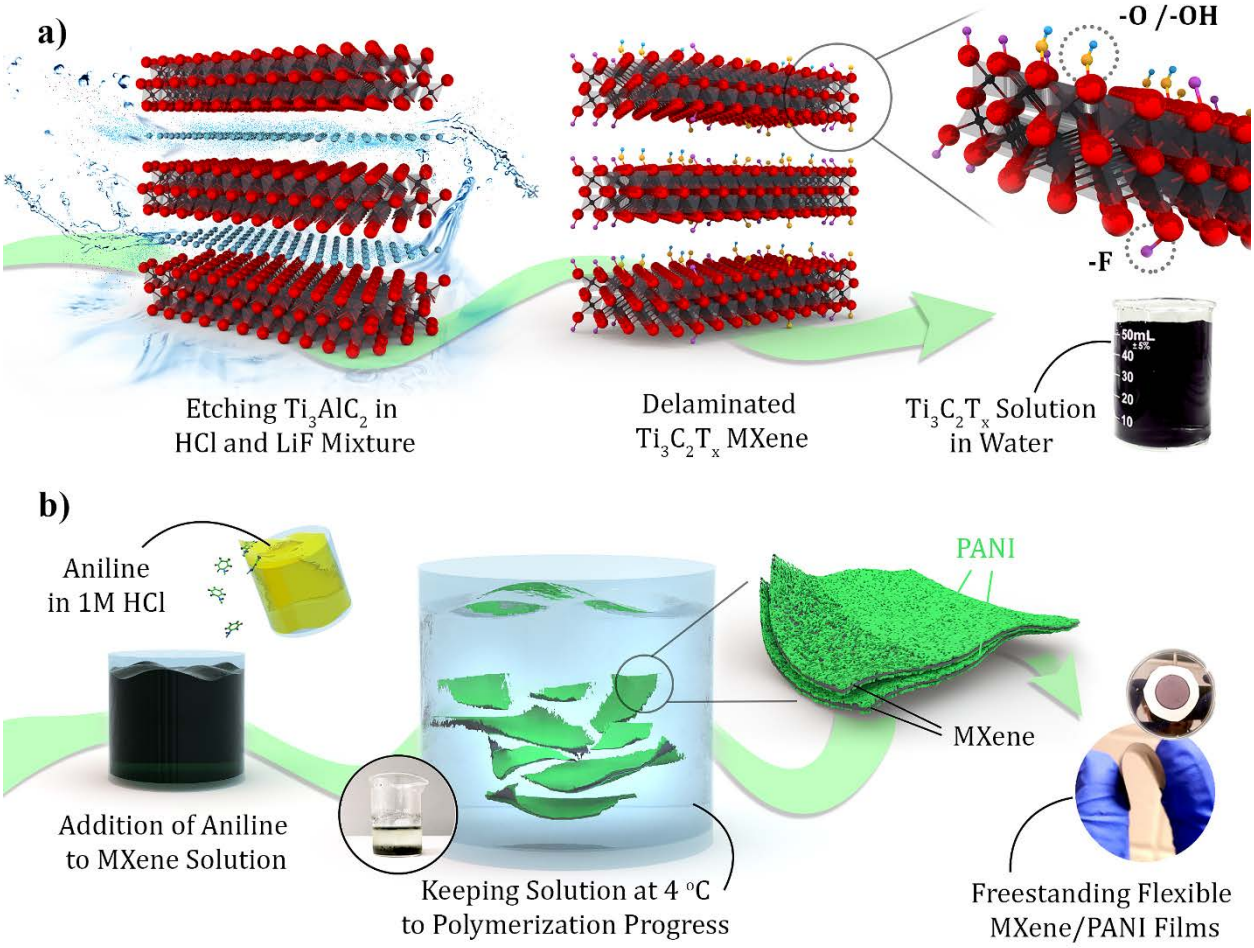

Figure 1. (a) Schematic illustration of the synthesis of $Ti_3C_2T_x$ MXene by selective etching of Al layer for the structure of layered Ti_3AlC_2 MAX phase. After the synthesis the surface of $Ti_3C_2T_x$ is terminated with various functional groups. (b) Schematic representation of the process used for the synthesis of $Ti_3C_2T_x$/PANI hybrid electrodes.

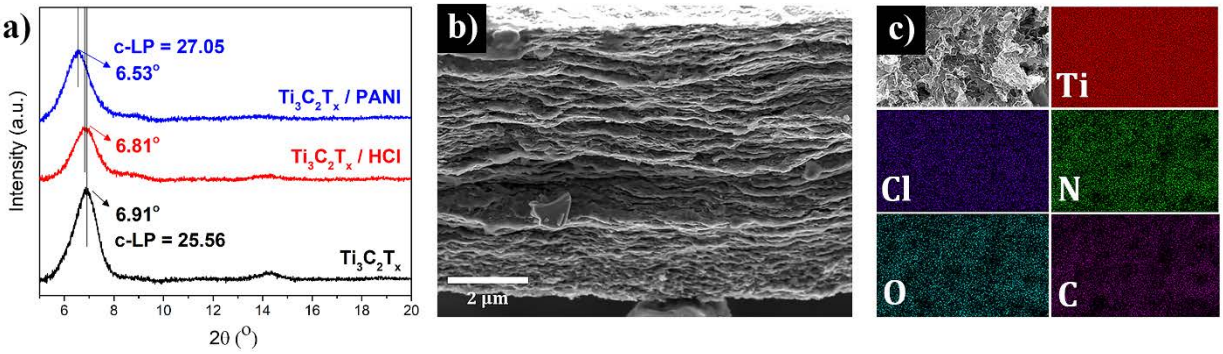

Figure 2. (a) XRD patterns of freestanding films of $Ti_3C_2T_x$, $Ti_3C_2T_x$ crumpled with HCl, and Ti_3CT_x/PANI hybrids films. The (0002) peak of the MXene shifts from 6.91º to about 6.53º as a result of PANI deposition on MXene flakes. (b) A cross-sectional SEM image of the fabricated hybrid films. (c) EDS mapping of Ti_3CT_x/PANI electrodes showing presence of N from the deposited PANI along with Ti, Cl, O and C from $Ti_3C_2T_x$.

mixture solution results in the flocculation of a hybrid material. As shown in Fig. 1b, the color of supernatant in the MXene/aniline mixture solution is clear in contrast to the yellowish color of solution of aniline in HCl. The crumpled $Ti_3C_2T_x$/aniline solution was kept at a low temperature (~ 4 ºC) to complete the polymerization process. Then, the crumpled hybrid material was dispersed in water by hand-shaking and used for fabrication of freestanding films through vacuum filtration. Our initial characterization of the synthesized materials (explained in detail in the ESI), showed that the amount of deposited PANI in the hybrid electrodes can be increased with increasing the amount of aniline in the synthesis solutions. However, the best electrochemical performance was achieved for samples with $Ti_3C_2T_x$ to aniline ratio of 1:2 (for simplicity referred to as $Ti_3C_2T_x$/PANI in the following). Therefore, samples prepared with this ratio of precursor materials were selected for detailed characterization. For comparison, freestanding films of pristine $Ti_3C_2T_x$ as well as $Ti_3C_2T_x$ sheets treated in 1 M HCl solutions were also prepared using the same fabrication method. It should be noted that addition of HCl solution to $Ti_3C_2T_x$ dispersions also results in crumpling of MXene flakes.[37] Fig. 2a shows the X-ray diffraction (XRD) patterns of the films prepared using $Ti_3C_2T_x$/PANI crumpled flakes, $Ti_3C_2T_x$ crumpled with HCl, and pristine $Ti_3C_2T_x$. As shown in this figure, for the $Ti_3C_2T_x$/PANI hybrid film the peak corresponding to the (0002) plane of MXene downshifts to about 6.53º from its position for the pristine $Ti_3C_2T_x$ (at around 6.9º). This corresponds to a 1.5 Å increase in the c-lattice parameter (c-LP) and 0.75 Å increase in the d-spacing after the PANI deposition. However, the calculated increase in d-spacing was only about 0.18 Å in case of the sample prepared after treatment in HCl solution. As expected, further increase in interlayer spacing was observed for samples synthesized using a higher ratio of

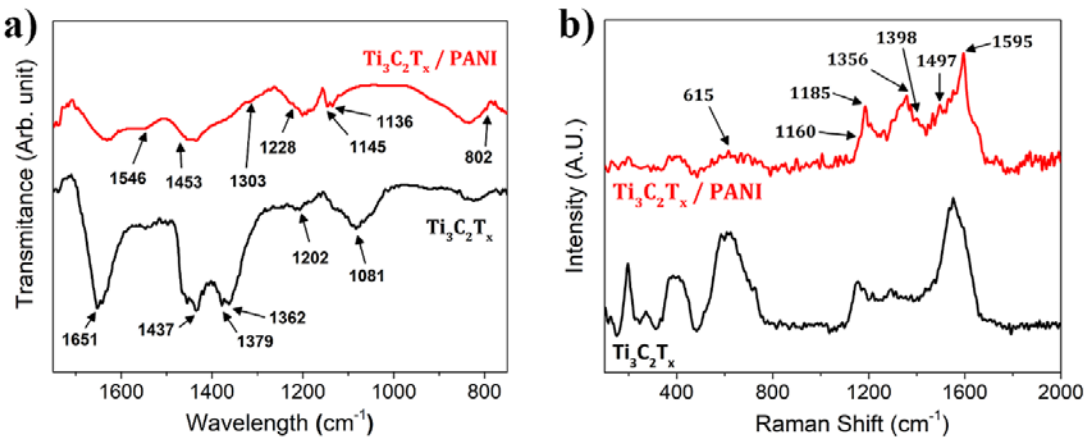

Figure 3. (a) FTIR spectra and (b) Raman Spectra of a delaminated $Ti_3C_2T_x$ film and a $Ti_3C_2T_x$/PANI hybrid film.

aniline and the largest increase in d-spacing (~6.12 Å) was observed for a sample prepared using a MXene to aniline ratio of 1:500 (Fig. S1). The cross-sectional scanning electron microscopy (SEM) image of a $Ti_3C_2T_x$/PANI film shows the layered structure formed during the directional assembly of the hybrid flakes using vacuum filtration (Fig. 2b). The energy dispersive spectroscopy (EDS) mapping of the top surface of the hybrid films showed the presence of nitrogen in the electrodes after PANI deposition. EDS also showed a decrease in the oxygen content of the MXene to 15.7 at.% from 25 at.% before PANI deposition (Table S1).

The Fourier transform infrared spectroscopy (FTIR) spectra of a $Ti_3C_2T_x$/PANI film and a pristine $Ti_3C_2T_x$ are shown in Fig 3a. After PANI deposition, the intensities of absorption bands corresponding to O, OH and F surface functional groups of $Ti_3C_2T_x$ (1651, 1437, 1379, 1362, and 1081 cm^{-1})[38,39] are decreased, which is consistent with the decrease in the measured F and O content shown by EDS. Furthermore, a few new bands appear in the spectrum of the hybrid films that suggest the deposition PANI on the surface of MXene sheets. These include the bands corresponding to C=C stretching vibrations of quinoid and benzenoid rings at 1546 and 1453 cm^{-1}, respectively, and the C-N stretching vibrations at 1303 and 1228 cm^{-1}. The bands corresponding to the C-H stretching of the aromatic amine apear at 1145 and 1136 cm^{-1} and the peak at 802 cm^{-1} can be assigned to aromatic C-H out-of-plane bending vibration.[40] Raman analysis of $Ti_3C_2T_x$/PANI hybrid films (Fig. 3b) showed decreased intensity of MXene peaks after PANI deposition as well as appearance of main characteristic peaks of PANI at 1160 and 1185 cm^{-1} (C-H stretching vibration of benzenoid ring), 1497 cm^{-1} (C=N stretching of quinoid ring), and 1595 cm^{-1} (C-C stretching of benzenoid ring).[29,35] Also, the two newly peaks observed at 1356 and 1398

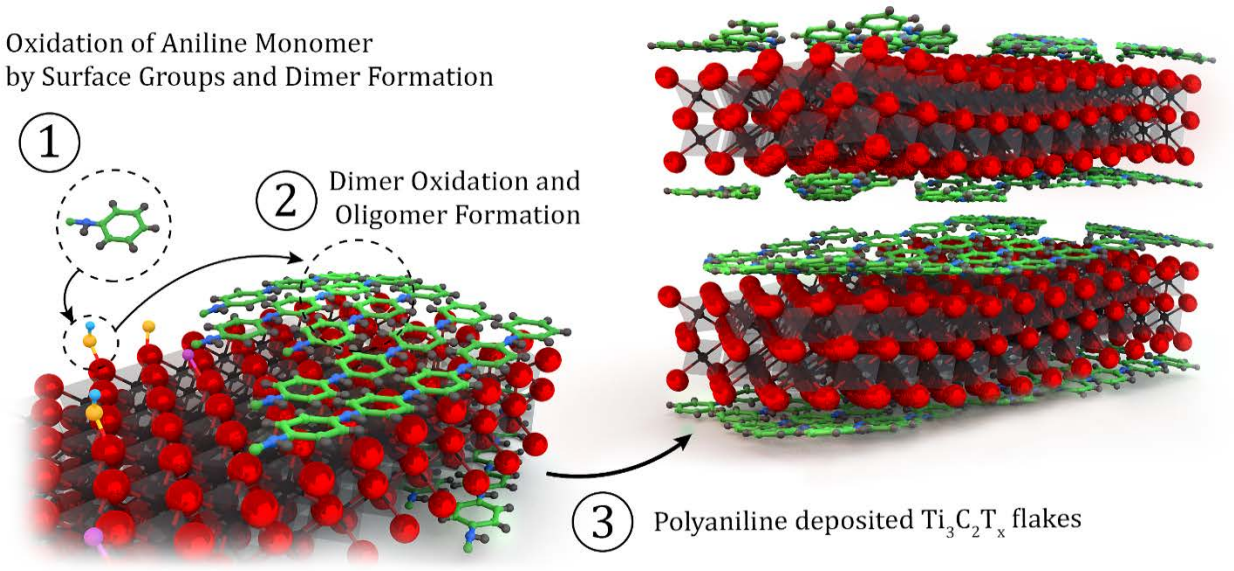

Figure 4. Suggested mechanism for polymerization of aniline on the surface of $Ti_3C_2T_x$ MXene. (1) Hydroxyl and oxygen surface groups initiate oxidation of aniline and the oxidation products form dimers at the surface of MXene. (2) Produced dimers are oxidized to form oligomers and polymers. (3) PANI is deposited on the surface of $Ti_3C_2T_x$ flakes.

cm^{-1} indicate the presence of PANI in its highly conductive emeraldine form.[35] Furthermore, atomic force microscopy (AFM) analysis of $Ti_3C_2T_x$ flakes before and after aniline polymerization (Fig. S3) confirmed the deposition of PANI on the MXene flakes.

We speculate that deposition of PANI on the surface of $Ti_3C_2T_x$ sheets follows the charge transfer induced polymerization mechanism previously proposed for the polymerization of EDOT on the surface of MXene.[28] Fig. 4 schematically shows the suggested mechanism for the polymerization of aniline on the surface of $Ti_3C_2T_x$ flakes. Polymerization starts after the oxidation of aniline by the oxygen and hydroxyl functional groups present on the surface of $Ti_3C_2T_x$, which produces aniline cation radicals and/or neutral radicals.[34,41] The oxidation of aniline is the rate-liming step of the polymerization and after its completion the polymerization process can continue by the electrophilic substitution of the hydrogen atom in the benzene rings of the oxidation products to form aniline dimers. Since oxidation potential of produced dimers is much lower than that of aniline monomer, upon formation, the dimers can quickly oxidize and react with other aniline monomers through subsequent oxidation or deprotonation to form oligomers and polymer.[41]

The electrochemical characterization of the fabricated hybrid films was performed using a three-electrode setup with glassy carbon current collectors in 3M H_2SO_4 solution as the electrolyte (schematically shown in Fig. S4). Glassy carbon electrodes have a large overpotential for hydrogen evolution reaction and using these electrodes instead of the more commonly used stainless steel

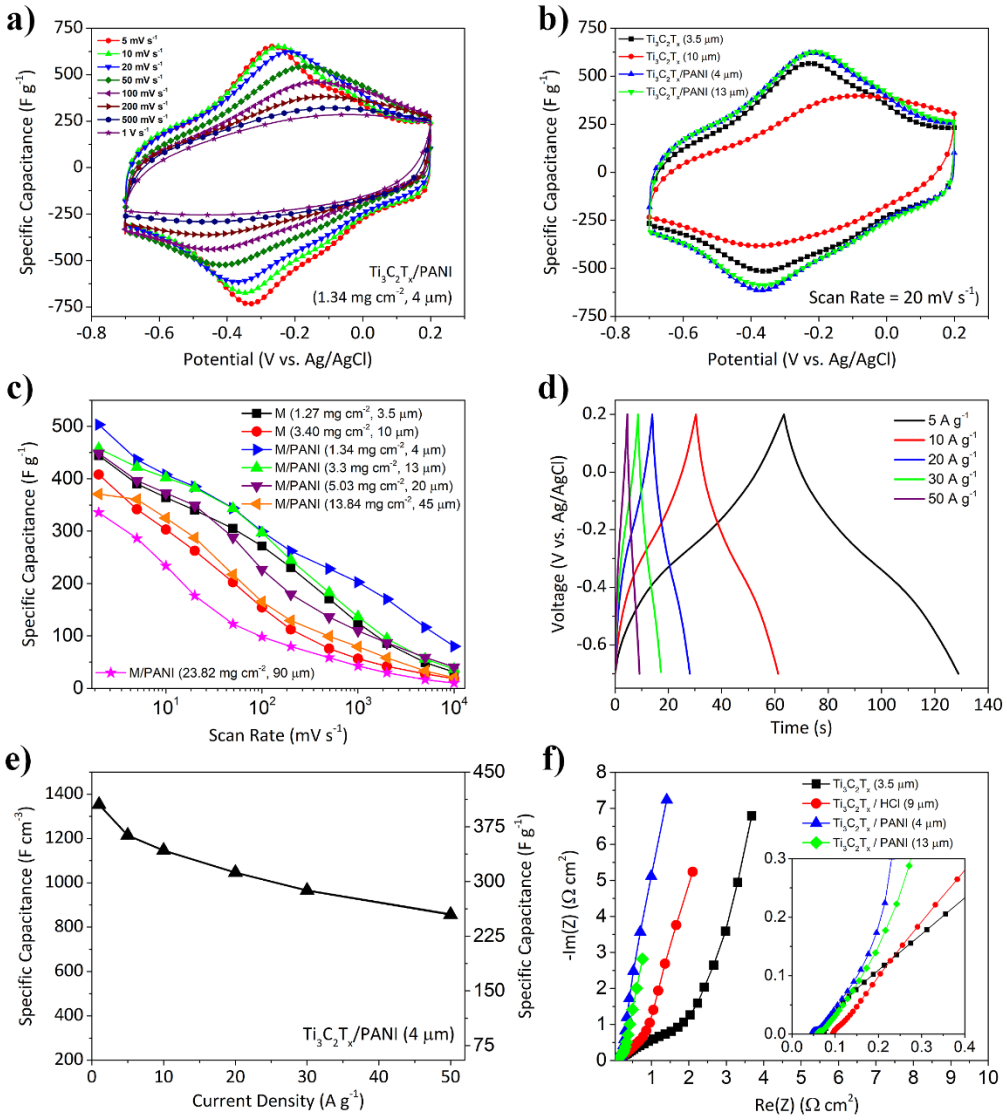

Figure 5. (a) Cyclic voltammetry (CV) curves of a freestanding $Ti_3C_2T_x$/PANI electrode (4 μm thickness) at scan rates of 5 mV s^{-1} to 1,000 mV s^{-1} in 3M H_2SO_4 electrolyte. (b) Comparison of the CV profiles of two $Ti_3C_2T_x$/PANI electrodes (4 and 13 μm thicknesses) and two pristine $Ti_3C_2T_x$ electrodes (3.5 and 10 μm thickness). (c) Gravimetric capacitance of electrodes with different thicknesses and mass-loadings. M represents pristine $Ti_3C_2T_x$ electrodes and M/PANI indicates a hybrid $Ti_3C_2T_x$/PANI electrode. (d) Galvanostatic charge/discharge profiles of $Ti_3C_2T_x$/PANI (4 μm thickness) electrode at different current densities of 1, 5, 10, 20, 30, and 50 A g^{-1}. (e) Specific capacitances of the $Ti_3C_2T_x$/PANI electrode (4 μm thickness) at different current densities. (f) Electrochemical impedance spectroscopy data for hybrid $Ti_3C_2T_x$/PANI electrodes (4 and 13 μm thicknesses), $Ti_3C_2T_x$/HCl, and $Ti_3C_2T_x$ electrodes, showing improved ion transport and lower resistance of$Ti_3C_2T_x$/PANI electrodes.

current collectors allows accessing a larger operating potential window for $Ti_3C_2T_x$ in the sulfuric acid electrolytes.[8] Fig. 5a shows cyclic voltammetry (CV) profiles of a freestanding $Ti_3C_2T_x$/PANI electrode with a thickness of ~4 μm (mass loading of 1.34 mg cm^{-2}) collected at scan rates ranging from 5 mV s^{-1} to 1,000 mV s^{-1}. The CV curves recorded at low scan rates show the signature redox peaks of $Ti_3C_2T_x$ and, as expected, at higher scan rates the redox peaks become broader. At a scan rate of 2 mV s^{-1}, a specific capacitance of ~503 F g^{-1} (or ~1682 F cm^{-3}) was calculated for the $Ti_3C_2T_x$/PANI hybrid electrode. To the best of our knowledge, this is the highest capacitance value reported for MXene-based electrodes to date and surpasses those previously reported for MXene/rGO and MXene hydrogel electrodes with comparable electrode thicknesses.[8,25] In addition, the $Ti_3C_2T_x$/PANI electrode showed a very high rate-handling capability. An electrode tested at various scan rates retained about 60% (~300 F g^{-1}, 1,000 F cm^{-3}) and 40% (~203 F g^{-1}, 677 F cm^{-3}) of its low scan rate capacitance at higher scan rates of 100 mV s^{-1} and 1,000 mV s^{-1}, respectively (Fig. 5c). Even at an extremely high scan rate of 10 Vs^{-1}, the hybrid electrode showed a capacitance of ~80 F g^{-1}.

The high specific capacitance and excellent rate-handling capability of the $Ti_3C_2T_x$/PANI films can be explained by the increase in the interlayer spacing of MXene sheets in the structure of the hybrid electrodes. This facilitates the ion transport inside the electrode structure and increases the electrolyte's ions (protons) accessibility to the redox-active sites at the surface of $Ti_3C_2T_x$. It is important to note that PANI does not directly contribute to charge storage in the fabricated electrodes as it is electrochemically inactive in the potential window that $Ti_3C_2T_x$ is active. Therefore, in the fabricated electrodes PANI only act as a conductive spacer that improves the ionic and electronic conductivity of the electrodes. However, conductive polymers such as PANI are a much more effective conductive spacer compared to carbon nanomaterials (such as CNT) that are commonly used in design and fabrication of freestanding electrodes based on 2D materials.[27,28] The amount of PANI deposited on the MXene sheets can be precisely controlled by controlling the $Ti_3C_2T_x$ to aniline ratio during the synthesis of hybrid sheets. This allows preventing the restacking of the $Ti_3C_2T_x$ sheets by depositing a very thin layer of PANI on their surface and reducing the amount of the inactive component (dead weight) in the electrodes. For example, the amount of PANI in the hybrid $Ti_3C_2T_x$/PANI electrodes (synthesized using 1:2 MXene to aniline ratio) is only about ~3.2 wt.% (please see Fig. S9 in the SI for the result of thermogravimetric analysis (TGA)), but even this small amount of PANI is enough to increase the

interlayer spacing of the MXene sheets and substantially improve the electrochemical properties of the electrodes.

The improved ionic and electronic conductivity of the electrodes after PANI deposition allows fabrication of electrodes with much higher thicknesses and mass loadings compared to what is normally achieved for freestanding electrodes of 2D materials. Fig. 5b compares the CV curves of two $Ti_3C_2T_x$/PANI electrodes with thicknesses of 4 µm and 13 µm to CV curves of two pristine $Ti_3C_2T_x$ electrode with thicknesses of 3.5 µm and 10 µm at a scan rate of 20 mV s^{-1}. Increasing the thickness of the pristine $Ti_3C_2T_x$ films from 3.5 µm (mass loading of 1.27 mg cm^{-2}) to 10 µm (mass loading of 3.4 mg cm^{-2}) resulted in a significant loss of capacitance (from 340 F g^{-1} to 262 F g^{-1}). This observation is in agreement with previous reports on the effects of thickness on the performance of freestanding MXene electrodes.[20] In contrast, in the case of $Ti_3C_2T_x$/PANI films, the electrode with 13 µm thickness (mass loading of 3.3 mg cm^{-2}) showed a pseudocapacitive response similar to the one with 4 µm thickness and delivered an almost equal gravimetric capacitance of ~383 Fg^{-1} at 20 mV s^{-1} (~385 F g^{-1} for the 4 µm thick electrode). The calculated specific capacitance of the 13 µm thick $Ti_3C_2T_x$/PANI electrode is higher than the capacitance of both 3.5 µm and 10 µm thick pristine MXene electrodes by about 13% and 47%, respectively. These results clearly show that the performance of the hybrid electrodes is much less thickness-dependent compared to pristine $Ti_3C_2T_x$ electrodes. Fig. 5c shows the rate-dependence of gravimetric capacitance of $Ti_3C_2T_x$/PANI electrodes with different thicknesses and mass loadings. The hybrid electrodes with the thicknesses of 4 µm and 13 µm show very similar rate-dependent behavior as their capacitance drops at higher CV scan rates. Both electrodes show a higher capacitance compared to the pristine MXene electrodes at all scan rates. More importantly, the specific capacitance of hybrid electrode with a thickness of 20 µm is almost similar to that of 3.5 µm thick $Ti_3C_2T_x$ electrode at almost all scan rates (Fig. 5c). Also, the performance of a hybrid electrode with thickness of ~45 µm is similar to the performance of 10 µm thick $Ti_3C_2T_x$ electrodes at all scan rates. Both electrode show a specific capacitance of about 325 F g^{-1} at 10 mV s^{-1}. As shown in Fig. 5c even at a very high thickness of ~90 µm, the fabricated hybrid electrodes still show much higher capacitance values compared to conventional supercapacitor electrodes based on activated carbon and other porous carbon materials.[42]

Fig. 5 d and e show charge-discharge profiles of the 4 µm thick $Ti_3C_2T_x$/PANI electrode at current densities ranging from 5 to 50 A g^{-1}. The charge/discharge profiles are typical of Ti_3C_2Tx

electrodes with near triangular shapes and broad humps that indicate the pseudocapacitive response of the material. The 4 μm $Ti_3C_2T_x$/PANI film could deliver a volumetric capacitance of about 1353 F cm^{-3} at 1 A g^{-1} and retains about 64% of its capacitance at a very high current density of 50 A g^{-1}. Fig. 5f shows the results of electrochemical impedance spectroscopy (EIS) performed on $Ti_3C_2T_x$/PANI electrodes of various thicknesses as well as a pristine $Ti_3C_2T_x$ electrode and an electrode assembled using $Ti_3C_2T_x$ crumpled by HCl treatment. Nyquist plots of both 4 μm and 13 μm hybrid films show the low ion transport resistance of the electrodes with near vertical rise of the imaginary impedance at low frequencies. However, for the 3.5 μm thick $Ti_3C_2T_x$, the 45-degree linear part of the impedance (Warburg impedance related to ion transport resistance) is much larger compared to hybrid electrodes. The length of the Warburg region decreases for the electrodes fabricated using the HCl treated $Ti_3C_2T_x$, but it is still much larger than the same region in the hybrid electrodes.

Fig. 6a shows the logarithm of CV peak current versus the logarithm of the scan rate for various fabricated electrodes. This graph can be used to explain the kinetics of charge storage in the electrodes. Considering a power-law relationship between peak CV current, i_p, and scan rate, v, we can write:[43]

$$i_p = a v^b \qquad (1)$$

where a and b are adjustable variables. Therefore, a plot of $\log(i_p)$ vs. $\log(v)$ would be a straight line with a slope of b.[8,43] In equation 1, a b-value of 0.5 implies a diffusion-controlled charge storage mechanism while b=1 is representative of surface-controlled capacitive storage.[43] As it can be seen in Fig. 6a, for a 4 μm thick $Ti_3C_2T_x$/PANI film the b-value is close to 1 for scan rates up to 5 V s^{-1}. However, for the 13 μm and 20 μm thick hybrid electrode the b-value remains close to 1 up to a scan rate of 500 mV s^{-1}, whereas a 10 μm thick $Ti_3C_2T_x$ only showed capacitive behavior up to a scan rate of 50 mV s^{-1}. The fabricated hybrid electrodes also showed very good cycle life performance. As shown in Fig. 6b, a 20 μm thick $Ti_3C_2T_x$/PANI electrode retained 98.3% of it is initial capacitance after 10,000 cycles at a CV scan rate of 20 mV s^{-1}.

Further analysis of the charge storage mechanism of the fabricated electrodes was performed using the method explained by Wang et al.[44] to separate the contribution of surface-controlled and diffusion-controlled processes to their charge storage during CV experiments. Fig. 6c and d show the CV profiles of a 13 μm thick $Ti_3C_2T_x$/PANI electrode at scan rates of 2 and 20

mV s^{-1}, respectively. The hatched portions of graphs show the capacitive contributions (an

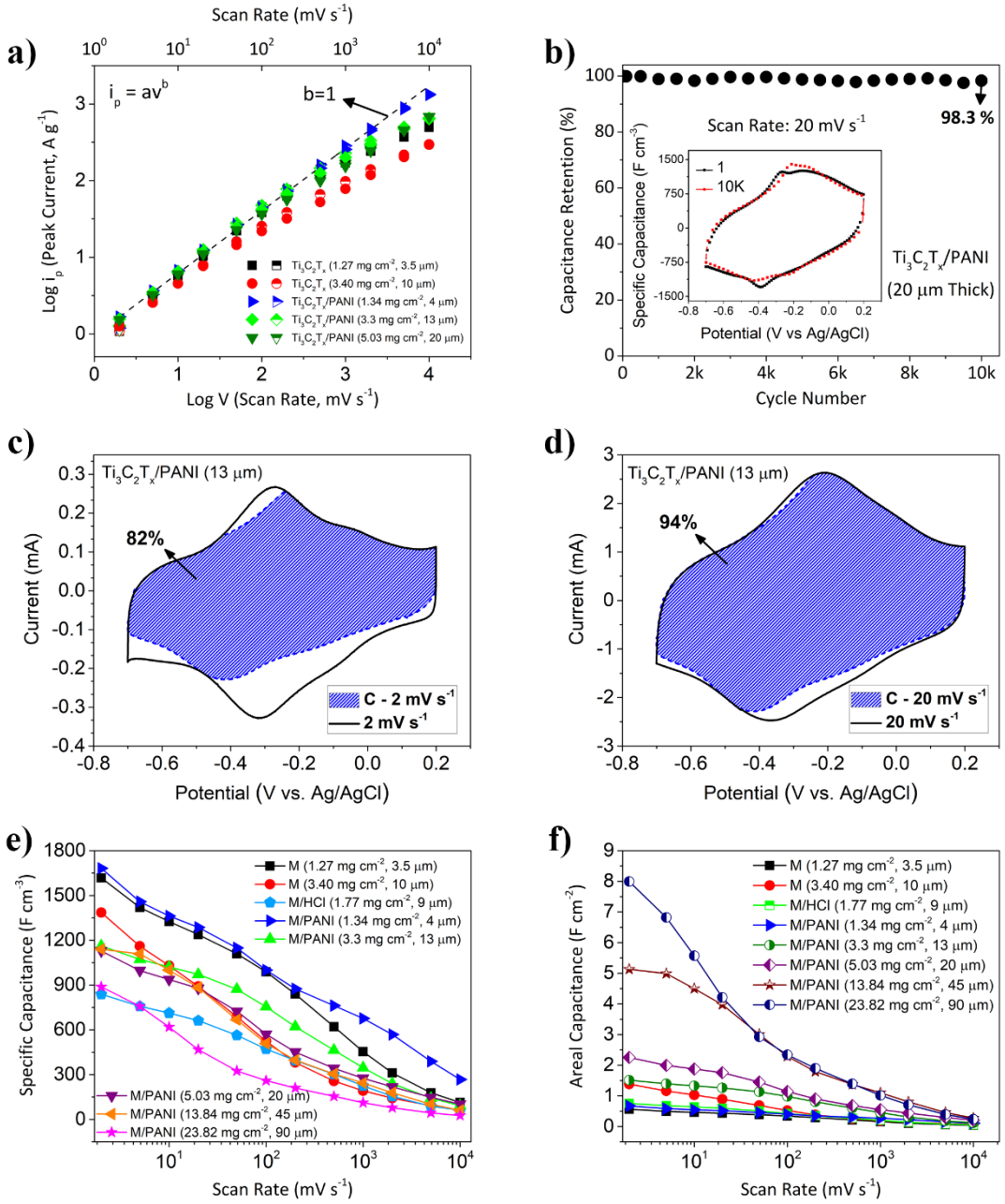

Figure 6. (a) Logarithm of cathodic (solid symbols) and anodic (half-filled symbols) peak currents versus logarithm of scan rate for various $Ti_3C_2T_x$/PANI electrodes for determination of b-values. (b) Cyclic performance of a 20 μm thick $Ti_3C_2T_x$/PANI hybrid electrode tested at a scan rate of 20 mV s^{-1} showing 98.3% capacitance retention after 10,000 cycles. Inset shows CV profiles before and after 10,000 cycling. CV curves of a $Ti_3C_2T_x$/PANI electrode (13 μm thickness) at (c) 2 mV s^{-1} and (d) 20 mV s^{-1}. The hatched portions of the graphs represent the contribution of surface-controlled processes (capacitive/pseudocapacitive) to the charge storage. (e) volumetric and (f) areal capacitance of pristine $Ti_3C_2T_x$ electrode (M) and hybrid $Ti_3C_2T_x$/PANI electrode (M/PANI) with different mass loading and thicknesses.

indication of charge storage mechanism with surface controlled redox reactions) to the total charge stored in the electrode at each scan rate.[20] At the lower scan rate of 2 mV s^{-1}, about 82% of the charge stored in the hybrid electrodes is due to capacitive contributions. As expected, as the scan rate is increased to 20 mV s^{-1} the contribution of the diffusion-limited processes decreases and about 94% of the capacitance stems from fast surface pseudocapacitance charge storage. It is worth noting that capacitive contribution was about 58% and 81% for a 10 µm thick $Ti_3C_2T_x$ electrode at scan rates of 2 and 20 mV s^{-1}, respectively (Fig. S6).

Fig. 6e shows the volumetric capacitances of various electrodes fabricated in this study. The addition of PANI and the increased interlayer spacing of MXene sheets lead to the lower density of the hybrid electrodes compared to the pristine $Ti_3C_2T_x$ electrodes. Therefore, the impact of PANI deposition on the volumetric capacitance of the electrodes is less than its impact on the gravimetric capacitance of the electrodes. As shown in Fig. 6f, $Ti_3C_2T_x$ and $Ti_3C_2T_x$/PANI electrodes with similar thickness show similar volumetric capacitances at different scan rates. Similar behavior was reported previously for microporous $Ti_3C_2T_x$ MXene electrodes.[8] Nevertheless, the PANI deposited hybrid electrodes showed compelling volumetric capacitances even at very high thicknesses. As shown in Fig 6e, the hybrid electrodes with thicknesses of 13 µm (3.3 mg cm^{-2}) , 20 µm (5.03 mg cm^{-2}), and 90 µm (23.82 mg cm^{-2}) showed excellent volumetric capacitances of about 1163 F cm^{-3}, 1129 F cm^{-3}, and ~889 F cm^{-3} (~47% less than the capacitance of 4 µm thick $Ti_3C_2T_x$/PANI electrode) at a scan rate of 2 mV s^{-1}, respectively. Therefore, an important advantage of synthesized hybrid materials over the pristine $Ti_3C_2T_x$ is that they can be used for fabrication of very thick electrodes. This is a critical property since in many perceived applications of advanced ECs, such as energy storage in wearable and portable devices and self-powered microsystems, there is a limited area available for the device and increasing the electrode thickness can enhance the energy density.[45] Therefore, materials that can be assembled in thick electrodes and still show high specific capacitance are highly desirable for these applications. The hybrid $Ti_3C_2T_x$/PANI electrode could be an excellent option for devices fabricated in a limited footprint area as high thickness of the electrodes increases their areal capacitance (capacitance normalized by the geometric area of the electrode). For example, an areal capacitance of about 2.26 F cm^{-2} was calculated for the 20 µm thick hybrid electrode (5.03 mg cm^{-2} mass loading) at 2 mV s^{-1} (Fig. 6f). Moreover, an electrode with thickness of ~90 µm (23.82 mg cm^{-2} mass loading) delivered an unprecedented areal capacitance of ~8 F cm^{-2} at 2 mV s^{-1} (~1 F cm^{-2} at 1 V s^{-1}),

exceeding the performance of previously reported microporous and hydrogel MXene electrodes (~ 4 F cm^{-2}).[8]

We also prepared symmetric supercapacitors using $Ti_3C_2T_x$/PANI (4 μm) electrodes to evaluate the performance of the electrodes in full cells. CV curves and specific capacitances of the symmetric supercapacitor (in 3M H_2SO_4) are shown in Fig. S10. The symmetric cell showed specific capacitances of ~130 F g^{-1} and ~575 F cm^{-3} (considering the total weight and volume of the active materials) at a scan rate of 2 mV s^{-1}. The symmetric supercapacitor based on $Ti_3C_2T_x$/PANI could deliver an ultrahigh energy density of 79.8 Wh L^{-1} at a power density of ~ 575 W L^{-1} (Ragone plots are shown in Fig. S11), surpassing the previously reported values for MXene/rGO symmetric supercapcaitors.[25]

4. Conclusions

In summary, we have demonstrated the fabrication of high performance MXene/PANI hybrid electrodes through an oxidant-free *in situ* polymerization process. The freestanding hybrid electrodes were fabricated by vacuum filtration of hybrid sheets and showed an increased interlayer spacing compared to the films fabricated using pristine $Ti_3C_2T_x$. Both thin and thick $Ti_3C_2T_x$/PANI hybrid electrodes showed significantly enhanced pseudocapacitive charge storage compared to the pristine $Ti_3C_2T_x$ electrodes. The thinner $Ti_3C_2T_x$/PANI electrodes showed very high capacitances of about 503 F g^{-1} and 1682 F cm^{-3} at 2 mV s^{-1} scan rate. The most important impact of PANI deposition on the performance of the electrodes was enhancing the ion transport properties of the electrodes. Consequently, the thickness and mass loading of the hybrid electrodes could be increased without a severe impact on their performance. We demonstrated that even a very thick electrode (~45 μm thickness) prepared using $Ti_3C_2T_x$/PANI hybrid sheets could deliver specific capacitances of about 371 F g^{-1} (1141 F cm^{-3}) and 287 F g^{-1} (884 F cm^{-3}) at scan rates of 2 mV s^{-1} and 20 mV s^{-1}, respectively. With a capacitance retention of over 98% after 10,000 cycles and areal capacitance of up to 8 F cm^{-2}, the performance of the fabricated $Ti_3C_2T_x$/PANI hybrid electrodes matches or surpasses the state-of-the-art EC electrodes based on carbon nanomaterials and previously reported MXene electrodes.[8,20,25,27]

ACKNOWLEDGMENTS

This work was partially supported by Alabama EPSCoR Research Seed Grant Program. We also acknowledge support by the startup funds and intramural grants program (IGP) at Auburn University. A.V.M. acknowledges the support from Alabama EPSCoR Graduate Research Scholar Program (GRSP Round 11 and 12) doctoral fellowship. J. O. also acknowledges the support from GRSP round 12 doctoral fellowship. Authors thank Matthew Noor for helping with the TGA experiments. We thank Auburn University's Department of Biosystems Engineering for providing access to FTIR characterization tool.

Conflict of Interest

The authors declare no conflict of interest.

Electronic Supplementary Information

ESI is available online and free of charge.

REFERENCES

1 X. Wang, Q. Weng, Y. Yang, Y. Bando and D. Golberg, *Chem. Soc. Rev.*, 2016, **45**, 4042–4073.
2 L. Yang, S. Wang, J. Mao, J. Deng, Q. Gao, Y. Tang and O. G. Schmidt, *Adv. Mater.*, 2013, **25**, 1180–1184.
3 Z. Yu, L. Tetard, L. Zhai and J. Thomas, *Energy Environ. Sci.*, 2015, **8**, 702–730.
4 M. R. Lukatskaya, O. Mashtalir, C. E. Ren, Y. Dall'Agnese, P. Rozier, P. L. Taberna, M. Naguib, P. Simon, M. W. Barsoum and Y. Gogotsi, *Science*, 2013, **341**, 1502–5.
5 Y. Xia, T. S. Mathis, M. Zhao, B. Anasori, A. Dang, Z. Zhou, H. Cho, Y. Gogotsi and S. Yang, *Nature*.
6 P. Simon and Y. Gogotsi, *Nat. Mater.*, 2008, **7**, 845–854.
7 B. Anasori, M. R. Lukatskaya and Y. Gogotsi, *Nat. Rev. Mater.*, 2017, **2**, 16098.
8 M. R. Lukatskaya, S. Kota, Z. Lin, M. Zhao, N. Shpigel, M. D. Levi, J. Halim, P. Taberna, M. W. Barsoum, P. Simon and Y. Gogotsi, *Nat. Energy*, 2017, **17105**, 1–6.
9 A. Vahidmohammadi, A. Hadjikhani, S. Shahbazmohamadi and M. Beidaghi, *ACS Nano*, 2017, **11**, 11135–11144.
10 X. Wang, S. Kajiyama, H. Iinuma, E. Hosono, S. Oro, I. Moriguchi, M. Okubo and A. Yamada, *Nat. Commun.*, 2015, **6**, 6544.
11 O. Mashtalir, M. Naguib, V. N. Mochalin, Y. Dall'Agnese, M. Heon, M. W. Barsoum and Y. Gogotsi, *Nat. Commun.*, 2013, **4**, 1716.
12 E. Lee, A. VahidMohammadi, B. C. Prorok, Y. S. Yoon, M. Beidaghi and D.-J. Kim, *ACS Appl. Mater. Interfaces*, 2017, **9**, 37184–37190.
13 S. J. Kim, H.-J. Koh, C. E. Ren, O. Kwon, K. Maleski, S.-Y. Cho, B. Anasori, C.-K. Kim, Y.-K. Choi, J. Kim, Y. Gogotsi and H.-T. Jung, *ACS Nano*, 2018, **12**, 986–993.
14 F. Shahzad, M. Alhabeb, C. B. Hatter, B. Anasori, S. Man Hong, C. M. Koo and Y. Gogotsi, *Science*

(80-.)., 2016, **353**, 1137–1140.
15 W. Bao, X. Tang, X. Guo, S. Choi, C. Wang, Y. Gogotsi and G. Wang, *Joule*, 2018, **3**, 1–10.
16 M. Naguib, O. Mashtalir, J. Carle, V. Presser, J. Lu, L. Hultman, Y. Gogotsi and M. W. Barsoum, *ACS Nano*, 2012, **6**, 1322–1331.
17 M. Naguib, V. N. Mochalin, M. W. Barsoum and Y. Gogotsi, *Adv. Mater.*, 2014, **26**, 992–1005.
18 M. Naguib, R. R. Unocic, B. L. Armstrong and J. Nanda, *Dalt. Trans.*, 2015, **44**, 9353–9358.
19 B. Anasori, Y. Xie, M. Beidaghi, J. Lu, B. C. Hosler, L. Hultman, P. R. C. Kent, Y. Gogotsi and M. W. Barsoum, *ACS Nano*, 2015, **9**, 9507–9516.
20 M. Ghidiu, M. R. Lukatskaya, M.-Q. Zhao, Y. Gogotsi and M. W. Barsoum, *Nature*, 2014, **516**, 78–81.
21 M. Zhao, C. E. Ren, Z. Ling, M. R. Lukatskaya, C. Zhang, K. L. Van Aken, M. W. Barsoum and Y. Gogotsi, *Adv. Mater.*, 2015, 339–345.
22 P. Hu, Y. Shen, Y. Guan, X. Zhang, Y. Lin, Q. Zhang and C. W. Nan, *Adv. Funct. Mater.*, 2014, **24**, 3172–3178.
23 A. Byeon, A. M. Glushenkov, B. Anasori, P. Urbankowski, J. Li, B. W. Byles, B. Blake, K. L. Van Aken, S. Kota, E. Pomerantseva, J. W. Lee, Y. Chen and Y. Gogotsi, *J. Power Sources*, 2016, 1–9.
24 Y. G. C. E. Ren, M.-Q. Zhao, T. Makaryan, J. Halim, M. Boota, S. Kota, B. Anasori, M. W. Barsoum, *ChemElectroChem*, 2016, **3**, 689–693.
25 J. Yan, C. E. Ren, K. Maleski, C. B. Hatter, B. Anasori, P. Urbankowski, A. Sarycheva and Y. Gogotsi, *Adv. Funct. Mater.*, 2017, **1701264**, 1701264.
26 S. Xu, G. Wei, J. Li, W. Han and Y. Gogotsi, *J. Mater. Chem. A*, 2017, 1–26.
27 M. Boota, B. Anasori, C. Voigt, M. Zhao, M. W. Barsoum and Y. Gogotsi, *Adv. Mater.*, 2015, 1–6.
28 C. Chen, M. Boota, X. Xie, M.-Q. Zhao, B. Anasori, C. E. Ren, L. Miao, J. Jiang and Y. Gogotsi, *J. Mater. Chem. A*, 2017, **00**, 1–6.
29 N. A. Kumar, H.-J. Choi, Y.-R. Shin, D. W. Chang, L. Dai and J.-B. Baek, *ACS Nano*, 2012, **25**, 1715–1723.
30 D. W. Wang, F. Li, J. Zhao, W. Ren, Z. G. Chen, J. Tan, Z. S. Wu, I. Gentle, G. Q. Lu and H. M. Cheng, *ACS Nano*, 2009, **3**, 1745–1752.
31 K. Zhang, L. L. Zhang, X. S. Zhao and J. Wu, *Chem. Mater.*, 2010, **22**, 1392–1401.
32 A. Lipatov, M. Alhabeb, M. R. Lukatskaya, A. Boson, Y. Gogotsi and A. Sinitskii, *Adv. Electron. Mater.*, 2016, **2**, 1600255.
33 M. Alhabeb, K. Maleski, B. Anasori, P. Lelyukh, L. Clark, S. Sin and Y. Gogotsi, *Chem. Mater.*, 2017, **29**, 7633–7644.
34 S. Bhadra, D. Khastgir, N. K. Singha and J. H. Lee, *Prog. Polym. Sci.*, 2009, **34**, 783–810.
35 J.-M. Jeong, B. G. Choi, S. C. Lee, K. G. Lee, S.-J. Chang, Y.-K. Han, Y. B. Lee, H. U. Lee, S. Kwon, G. Lee, C.-S. Lee and Y. S. Huh, *Adv. Mater.*, 2013, **25**, 6250–6255.
36 J. Xu, K. Wang, S. Z. Zu, B. H. Han and Z. Wei, *ACS Nano*, 2010, **4**, 5019–5026.
37 V. Natu, M. Clites, E. Pomerantseva and M. W. Barsoum, *Mater. Res. Lett.*, 2018, **6**, 230–235.
38 Q. Xue, H. Zhang, M. Zhu, Z. Pei, H. Li, Z. Wang, Y. Huang, Y. Huang, Q. Deng, J. Zhou, S. Du, Q. Huang and C. Zhi, *Adv. Mater.*, 2017, 1604847.
39 H. Wang, J. Zhang, Y. Wu, H. Huang, G. Li, X. Zhang and Z. Wang, *Appl. Surf. Sci.*, 2016, **384**, 287–293.
40 X. M. Feng, R. M. Li, Y. W. Ma, R. F. Chen, N. E. Shi, Q. L. Fan and W. Huang, *Adv. Funct. Mater.*, 2011, **21**, 2989–2996.
41 N. Gospodinova and L. Terlemezyan, *Prog. Polym. Sci.*, 1998, **23**, 1443–1484.
42 P. Simon and Y. Gogotsi, *Acc. Chem. Res.*, 2013, **46**, 1094–1103.
43 V. Augustyn, J. Come, M. a Lowe, J. W. Kim, P.-L. Taberna, S. H. Tolbert, H. D. Abruña, P. Simon and B. Dunn, *Nat. Mater.*, 2013, **12**, 518–22.
44 J. Wang, J. Polleux, J. Lim and B. Dunn, *J. Phys. Chem. C*, 2007, **111**, 14925–14931.
45 Y. G. Majid Beidaghi, *Energy Environ. Sci.*, 2014, **7**, 867–884.